-A11, -A24, -A26, -A31 or -A33; vi) an Eastern Cooperative Oncology Group performance status of 0-1, age between 20 and 75 years and adequate hematological function (white blood cell count ≥2,400/μl, hemoglobin level ≥8.0 g/dl and platelet counts ≥50,000/μl), renal function (serum creatinine ≤1.4 g/dl) and hepatic function (total bilirubin <2.5 mg/dl); and vii) negative status for hepatitis B antigens. The protocols for both series were approved by the Institutional Ethics Review Boards of Kurume University, and complete written informed consent was obtained from all patients at the time of enrollment. A total of 40 patients entered one of the two protocols at our institution between November 2003 and November 2008. In addition, the 39 patients who received more than six vaccinations were included in this follow-up study.

Peptides and vaccination. For the first protocol, four peptides capable of inducing both cytotoxic T lymphocyte (CTL) and humoral responses (IgG) in HLA-A24$^+$ patients were provided for vaccination as previously reported (11). These four peptides were derived from well-conserved regions of HCV1b as follows: protein E1-derived peptide from positions 213 to 221 (E1 213-221); protein E2-derived peptide from positions 488 to 496 (E2 488-496); non-structural region 3-derived peptide from positions 1081 to 1090 (NS3 1081-1090); and non-structural region 5A-derived peptide from positions 2132 to 2140 (NS5A 2132-2140). For the second protocol, we used a peptide for vaccination derived from HCV core protein; this peptide was capable of inducing both CTL and humoral responses (IgG) in nearly all HCV patients with different HLA-class IA alleles in Japan (12,14). This peptide originated from the HCV core protein at positions 35 to 44 (C 35-44), a well-known HLA-A2-restricted CTL epitope (15).

These five peptides were prepared under conditions of Good Manufacturing Practice by the American Peptide Company (San Diego, CA, USA). The peptide emulsion was injected into the subcutaneous region of the side of the abdomen or upper arm every 2 weeks from the 1st to the 24th vaccination, every 3 weeks from the 25th to the 48th vaccination and every 4 weeks thereafter. The first cycle consisted of six vaccinations; a second cycle of six vaccinations was conducted with patient consent in cases lacking any signs of severe toxicity. When patients wished to continue with the course of vaccinations, the series was extended, unless either disease progression or severe toxicity was observed.

Humoral responses to peptides. Peptide-specific IgG levels in the blood samples were measured using Luminex® systems as reported previously (11). Briefly, diluted plasma samples were incubated with peptide-coated microspheres. After the microspheres were washed, they were incubated with various antibodies (anti-human-IgG, -IgA, -IgM, -IgE, -IgG1, -IgG2, -IgG3 and -IgG4; purchased from Vector, Bethyl, Vector, Biosource, The Binding Site Ltd., Cappel, Cappel and The Binding Site Ltd., respectively). After being washed, the microspheres bound to each antibody were reacted with biotin-labeled detection antibody (Zymed or Cappel) and the corresponding R-phycoerythrin (Invitrogen) antibody, and the antibody levels were detected by a Luminex system as reported previously (11). All pre- and post-vaccination samples were measured simultaneously in order to avoid any possible biases associated with the *in vitro* assay. IgG against recombinant HCV core protein was also measured by means of a commercially available radioimmunoassay kit (SRL Laboratory, Tokyo, Japan).

Clinical laboratory data. Clinical laboratory values (e.g., serum ALT and AFP levels and blood platelet numbers) were measured by the Clinical Laboratory Division of the Kurume University Hospital. Quantitation of HCV-RNA, based on quantitative reverse transcription-polymerase chain reaction (qRT-PCR), was performed by a clinical lab company (SRL Laboratory).

Results

Patient characteristics and clinical responses. Thirty-nine HCV-positive patients (33 CH and 6 LC) who had received more than six rounds of HCV-derived peptide vaccinations were included in the analysis (Tables I-III). All patients, with the exception of 1 (pt. 16, HCV2a), were infected with HCV1b. At the time of entry into the study, 35 patients were non-responders to interferon-based therapy, and the remaining 4 patients refused treatment. All 6 LC patients had a history of HCC treatment, while 3 CH patients had space-occupying hepatic lesions (SOLs) suspected of being cancerous at the time they entered the study. The median frequency of vaccination was 26 rounds (range 6-89), and the median duration of the vaccination period was 16 months (range 2-69). No severe toxicity was observed throughout the vaccination period, but grade 1 or 2 local inflammation at the injection site was observed in most cases. Twelve patients were still receiving vaccinations at the time of this writing (September 2009), and the course of vaccinations had been terminated in the remaining 27 patients. Eleven patients received IFN-based therapy combined with vaccination followed by the vaccination alone, and 9 patients received IFN-based therapy after the end of vaccination (Tables I-III).

A significant decrease in ALT level (<70% ALT level at the end of vaccination or at the time of last vaccination vs. that before vaccination) was observed in 11 of 39 patients (7 of 28 patients treated with vaccination alone and 4 of 11 patients treated with vaccination alone followed by combined IFN-based therapy with vaccination). No significant decrease in platelet number (<70% at the end of vaccination or at the time of last vaccination vs. that before vaccination) was found in any of the 28 patients who received vaccination alone, but an increase (>130%) was noted in 1 patient. By contrast, a decrease in platelet number was observed in 4 of 11 patients with vaccination alone followed by combined IFN therapy. A significant decrease in the AFP level was found in 1 of 28 patients who received vaccination alone, whereas it was observed in 4 of 9 patients with vaccination alone followed by combined IFN therapy. HCV-RNA responders with >1 log decline were not found among the 28 patients who received the vaccination alone, while 4 of 11 patients who had received vaccination followed by combination therapy, including 3 sustained viral responders (SVR; pt. 1, 8 and 15), were HCV-RNA responders. As post-vaccination treatment, 9 patients received IFN-based therapy and only 1 (pt. 23) reached the status of SVR. The median observation period of the 39 patients was 47 months (range 10-69).

Table I. Patient characteristics before vaccination.

Patient	Age	Gender	Disease	Previous IFN	ALT	Plt	AFP	HCV-RNA
1	38	M	CH	-	139	11	8	465
2	43	M	CH (SOL)	IFN+RBV	139	17	9	3,820
3	52	F	LC (post HCC)	IFN+RBV	105	9	173	651
4	65	M	LC (post HCC)	IFN+RBV	292	5	7	4,030
5	55	M	CH	IFN+RBV	119	9	11	4,290
6	42	M	CH	IFN+RBV	73	12	4	621
7	49	M	CH	IFN+RBV	48	13	3	1,010
8	53	F	CH	IFN+RBV	27	21	4	2,090
9	70	F	CH	IFN+RBV	38	12	12	2,200
10	66	M	CH	IFN+RBV	154	15	11	139
11	58	F	CH	IFN+RBV	51	11	17	4,590
12	50	F	CH	IFN+RBV	62	14	10	1,730
13	61	F	CH	IFN+RBV	77	11	33	91
14	51	M	CH	IFN	41	22	3	3,420
15	50	M	CH	IFN+RBV	206	11	74	500
16	71	M	CH	IFN+RBV	114	9	4	114
17	51	M	CH	IFN	60	14	5	892
18	60	M	CH	IFN+RBV	108	8	9	3,100
19	49	F	CH	IFN+RBV	129	16	44	2,480
20	38	M	CH	IFN+RBV	358	6	29	2,870
21	61	F	LC (post HCC)	IFN+RBV	53	9	131	1,670
22	58	M	LC (post HCC)	RFA, IFN	45	8	7	2,130
23	71	M	CH	IFN	46	13	2	4,520
24	70	M	CH	IFN+RBV	47	25	5	2,470
25	68	M	CH	IFN+RBV	37	17	4	2,260
26	64	M	CH (SOL)	IFN+RBV	60	13	13	3,630
27	70	M	CH (SOL)	IFN+RBV	51	24	4	591
28	62	F	CH	-	24	19	5	583
29	53	F	CH	IFN	34	23	4	4,370
30	63	F	CH	-	73	12	3	59
31	58	F	CH	IFN+RBV	66	10	8	2,790
32	63	F	CH	IFN+RBV	52	12	3	2,230
33	57	F	CH	IFN+RBV	55	11	9	2,340
34	58	F	CH	IFN	80	12	7	2,150
35	58	F	CH	IFN+RBV	47	12	11	16,000
36	61	M	LC (post HCC)	IFN+RVB	104	10	27	32,000
37	58	M	CH	-	83	15	6	20
38	60	M	CH	IFN+RBV	144	16	5	25,000
39	73	M	LC (post HCC)	IFN+RBV	42	12	66	3,200

HCV, hepatitis C virus; CH, chronic hepatitis; SOL, space occupying lesions; LC, liver cirrhosis; HCC, hepatocellular carcinoma; IFN, interferon; RBV, ribavirin; ALT, alanine aminotransferase (IU/l); Plt, platelet numbers (x10^4 ml); AFP, α-fetoprotein (mg/ml); HCV-RNA, (kIU/ml).

Development of HCC. Under the circumstances described above, HCC became detectable during the vaccination period in 2 of 3 CH patients (pt. 26 and 27) with SOLs prior to vaccination. By contrast, HCC was undetectable throughout the vaccination period in the remaining 36 patients without a SOL prior to vaccination. However, HCC was diagnosed in 4 of these 36 patients after the course of vaccination, i.e., in 2 CH patients at 46 and 29 months after the end of vaccination (pt. 5 and 9), and in 2 LC patients at 49 and 18 months after the end of vaccination (pt. 4 and 21). Three of these 4 patients received IFN-based therapy combined with vaccination (pt. 5), or after the end of vaccination (pt. 9 and 21) and showed no viral response (Tables I-III).

Antibody responses. We measured the patient IgG responses to each of the peptide vaccines in plasma samples before,

Table II. Patient characteristics during vaccination.

Patient	Rounds	Duration (m)	Later addition of IFN	ALT	Plt	AFP	HCV-RNA	Onset of HCC (m)
1	39	18	+	54	10	4	-	
2	30	14	+	125	6	7	623	
3	25	11	+	110	5	300	1,120	
4	24	10	-	179	7	6	3,380	
5	28	13	+	125	8	5	5,000	
6	13	6	-	37	14	3	5,000	
7	44	22	+	67	9	2	1,360	
8	46	23	+	12	17	2	(-)	
9	18	8	-	29	15	10	4,430	
10	17	7	-	176	15	NA	301	
11	11	5	-	51	12	8	2,590	
12	15	7	-	83	12	12	2,120	
13	33	21	+	86	11	31	303	
14	19	8	-	68	23	4	4,470	
15	38	17	+	71	6	38	-	
16	64	30	+	93	10	6	(+)	
17	89+	61	-	39	14	6	1,600	
18	35	16	-	51	10	8	3,470	
19	26	15	+	193	10	28	2,890	
20	43	41	+	262	6	22	16,000	
21	22	12	-	63	9	134	3,870	
22	28	20	-	26	7	12	8,000	
23	6	2	-	51	13	2	2,310	
24	39+	35	-	108	22	2	32,000	
25	15	8	-	32	19	3	1,540	
26	19	10	-	68	13	39	3,650	+ (10)
27	33	24	-	71	23	6	200	+ (24)
28	33+	28	-	24	20	3	1,600	
29	29+	28	-	39	27	3	10,000	
30	33+	28	-	39	13	2	80	
31	32+	26	-	67	11	7	4,000	
32	32+	25	-	67	11	4	16,000	
33	17	9	-	44	12	11	5,000	
34	25+	21	-	55	12	7	2,000	
35	16+	13	-	67	9	19	8,000	
36	10	16	-	120	11	28	16,000	
37	23+	16	-	49	16	7	40	
38	14+	14	-	162	13	7	25,000	
39	16+	10	-	42	13	59	3,200	

HCV, hepatitis C virus; HCC, hepatocellular carcinoma; IFN, interferon; ALT, alanine aminotransferase (IU/l); Plt, platelet numbers ($x10^4$ ml); AFP, α-fetoprotein (mg/ml); HCV-RNA, (kIU/ml). m, months.

during and at the end of the vaccination period in all 39 patients. Moreover, when possible, we measured the IgG responses in patients after the end of the series of vaccinations (n=10). Representative results of all 39 cases are shown in Fig. 1A-C. In the first protocol for HLA-A24$^+$ patients (n=13), an increase in anti-peptide IgG to E1 213-221, E2 488-496, NS3 1081-1090 and NS5A 2132-2140 peptides at the end of the peptide vaccination was observed in 0 of 7, 12 of 13, 4 of 13 and 9 of 13 patients who received the corresponding peptides, respectively (Fig. 1A). An increase in IgG reactive to at least one of the vaccination peptides was observed in all 13 patients. The increased IgG reactive to the E2-488 or NS5A-2132, but not to the NS3-1081 peptide, was sustained for 6, 6, 49, 46, 17, 9, 6 and 6 months when the samples after the end of vaccination from pt. 1, 2, 4-6 and 9-11 were provided for measurement.

Table III. Patient characteristics post vaccination.

Patient	Post-vaccination IFN	Total OP (m)	Onset of HCC (m)
1			69
2			67
3			66
4		+ (49)	64
5		+ (46)	63
6	+		59
7	+		57
8			56
9	+	+ (29)	50
10	+		49
11	+		47
12			58
13			57
14	+		50
15			64
16			62
17			61
18	+		58
19			57
20			52
21	+	+ (18)	39
22			28
23	+		35
24			35
25			32
26			34
27			29
28			28
29			28
30			28
31			26
32			25
33			22
34			21
35			11
36			21
37			21
38			14
39			10

HCC, hepatocellular carcinoma; IFN, interferon; OP, observation periods. m, months.

In the second protocol for patients with different HLA-A alleles, the C 35-44 peptide was used for vaccination in all 26 patients, and an increase in anti-peptide IgG at the end of the peptide vaccination was observed in 22 of these patients (Fig. 1B and C). Ig isotypes and IgG subclasses of anti-C 35-44 peptide were also subjected to analysis in order to address whether Th1- or Th2-type immune responses were induced by peptide vaccination in the 26 patients who received C 35-44 peptide vaccinations. We found that all Ig isotypes (IgM, IgA, IgG and IgE), as well as all IgG subclasses (IgG1 to IgG4), were augmented by vaccination in all 22 patients exhibiting elevated IgG. Four representative cases (pt. 12, 19, 22 and 27) are shown in Fig. 2.

These results indicate that IgG responses to E2 488-496, NS5A 2132-2140 and C 35-44 peptides were boosted in the majority of vaccinated patients, i.e., IgG responses to NS3 1081-1090 were boosted in half of the patients, whereas the IgG response to the E1 213-221 peptide was not boosted in any of the patients. These results are consistent with those reported previously using samples from our Phase I study (11,12).

Measurement of cellular responses using post-vaccination samples was not carried out in this study, primarily due to the limited number of available peripheral blood mononuclear cells, although an increase in cellular responses to at least one of the vaccinated peptides during the Phase I studies was observed in the majority of patients, as reported previously (11,12).

Development of HCC and antibody responses. We then addressed the relationship between the development of HCC and patient immune responses.

HCC became detectable during the course of vaccination in 2 of 3 CH patients (pt. 26 and 27) with SOLs prior to vaccination. In these two patients, humoral responses to the vaccinated peptides were well augmented in the post-vaccination samples (Figs. 1 and 2). In the other patient (pt. 2) with a SOL but without HCC, the humoral responses to the vaccinated peptides were also augmented (Fig. 1).

HCC was undetectable in the remaining 36 patients throughout the vaccination period, but it became detectable in 4 patients post-vaccination, i.e., in 2 CH patients at 46 and 29 months after the end of the vaccination (pt. 5 and 9), and in 2 LC patients at 49 and 18 months after the end of the vaccination (pt. 4 and 21). The development of HCC in these four cases was associated with a disappearance of vaccination-induced humoral responses. Namely, the IgG boosting effect reactive to NS3-1081 and NS5A-2132, but not to E2-488, disappeared in pt. 4 and 5 when HCC became detectable 49 and 46 months after the end of vaccination, respectively (Fig. 1A). The IgG boosting effect reactive to NS5A-2132 and E2-488 also disappeared in pt. 9 when HCC became detectable 29 months after the end of vaccination. Similarly, the IgG boosting effect to the C-35 peptide in pt. 21 disappeared by the time HCC developed, i.e., 18 months after the end of the vaccination period (Fig. 1B).

The results presented above suggest an association between HCC development and the weakening of boosted IgG responses to the peptides used for vaccination. We then addressed whether IgG responses to the HCV core protein had any association with HCC development in pt. 21, who received core protein-derived peptide C-35 (Fig. 3). The increase in IgG levels in response to the HCV core protein was reduced to the pre-vaccination baseline level at the time of HCC development. The IgG responses in the remaining 3 patients who did not receive the C-35 peptide were also measured. As expected, there was no association in these 3 patients between IgG titers raised against the HCV core protein and HCC development (Fig. 3).

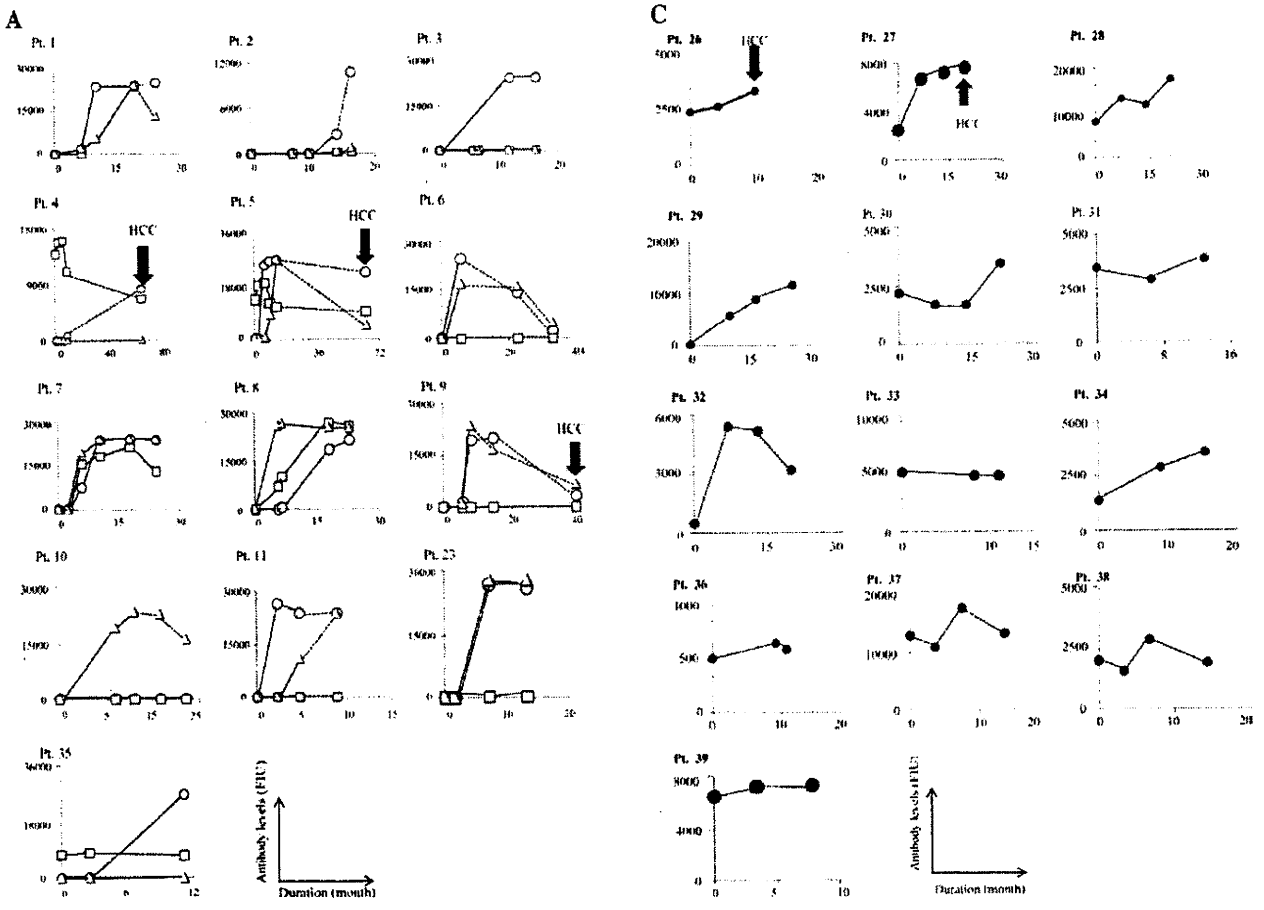

Figure 1. IgG responses to peptides. Kinetic measurement of IgG responses to each of the peptides used for vaccination in plasma samples before, during, and at the end of the vaccination period, as well as in samples obtained post-vaccination, when available. The vertical column indicates the levels of antibody expressed as fluorescence intensity units (FIU), as reported previously (11). The horizontal column indicates the duration of vaccination (——) and that of observation after the end of vaccination (-----). (A) o-o, IgG to E2 488-496; □-□, IgG to NS3 1081-1090; △-△, IgG to NS5A 2132-2140 peptides. (B and C) ●-●, IgG to C 35-44 peptide.

Discussion

The reported annual occurrence rates of HCC in CH patients, LC patients, non-responders and patients with a history of HCC treatment vary largely from <1-5, 5-8, 1-7 and 10-20% per year, respectively, depending on the population studied (5,16-22). HCC has been shown to develop even in sustained viral responders at a rate of <1-2% per year, depending on the population studied (23,24). Only 39 vaccinated patients were included in the present follow-up study; thus, information regarding general HCC occurrence and recurrence rates at the Kurume University Hospital could be useful for gaining a better understanding of the results of this study. The 2-year occurrence rate of HCC in non-vaccinated HCV1b$^+$ patients with platelet numbers of <130,000 per mm^3 (stages F3 and F4) (5) who failed to respond to IFN-ribavirin therapy was 19%, while the 2-year recurrence rate in non-vaccinated HCV1b$^+$ patients after a history of HCC treatment was 47.5% at Kurume University Hospital (Sata *et al*, unpublished data). In this study, 16 and 6 patients were matched to the former and

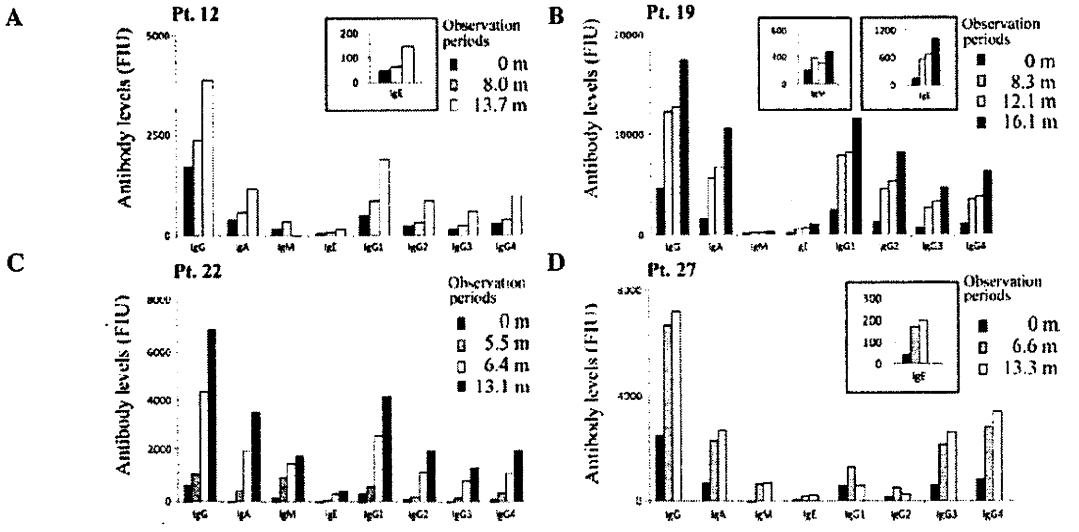

Figure 2. Isotypes and IgG subclasses. Kinetic measurement of Ig isotypes and IgG subclasses of anti-C 35-44 peptide was also studied in 22 patients. All isotypes (IgM, IgA, IgG and IgE), as well as all IgG subclasses (IgG1 to IgG4), were augmented by the C 35-44 vaccination in all 22 patients in whom IgG was elevated, as shown in Fig. 1. Four representative cases (pt. 12, 19, 22 and 27) are shown here.

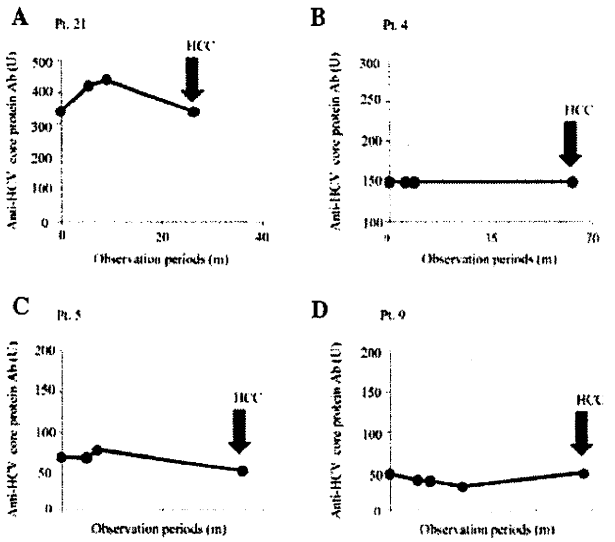

Figure 3. IgG responses to HCV core protein. Kinetic measurement of IgG responses against recombinant HCV core protein in plasma samples before, during and at the end of the vaccination, as well as after the end of vaccination in 4 patients who had developed HCC post-vaccination. The vertical column indicates the determined antibody level.

latter group of patients, respectively. A median observation period for these 22 patients after the initiation of vaccination was 55 months (range 10-69). HCC was undetectable in all of these 22 patients at least 30 months after the initiation of peptide vaccination. However, HCC became detectable 59, 58, 37 and 30 months after the initiation in pt. 4, 5, 9 and 21, respectively. With regard to post-vaccination, HCC became detectable at 49, 46, 29 and 18 months in pt. 4, 5, 9 and 21, respectively. These results suggest that peptide vaccination induced prophylaxis against HCC associated with HCV.

By contrast, HCC developed in 2 (pt. 26 and 27) of 3 CH patients with SOLs suspected of being cancerous at the start of the vaccination period (Tables I-III), suggesting that the peptide vaccine has no prophylactic effects in patients with pre-existing SOLs.

Our results suggest that the vaccination-induced increase in peptide-specific IgG lasts for 6 months after the end of a vaccination course. However, the duration of this response appears to depend on the specific peptides used for vaccination, as well as on the dose and frequency of vaccination. Thus, these issues need to be further investigated in future clinical trials with larger sample sizes. Moreover, HCC development was associated with a reduction in boosted immune responses showing reactivity to specific peptide vaccines, as well as to the corresponding core protein. Therefore, IgG reactivity to peptides used for vaccination may serve as a biomarker for predicting HCC development in HCV-positive patients who have received a peptide vaccine. It should be noted that only 4 patients were available for this aspect of the present study and therefore, further investigation is required in order to confirm our results. In addition, the biological roles of the peptide antibodies remain unclear at the present time and should be elucidated by future investigation.

Th1-type immune responses are thought to be involved in chronic-phase liver damage (25,26). Nelson *et al* found that interleukin-10 treatment resulted in the normalization of ALT levels in 19 of 22 CH patients who had been non-responders to INF-based treatment (27). Interleukin-10 promotes the production of IgA, IgG1 and IgG3 (28,29). We demonstrated an increase in all three of these Ig isotypes in post-vaccination samples, suggesting that the Th2-type immune response is indeed boosted by vaccination.

We also measured the CTL activity of PBMCs during the course of vaccination; our results were reported elsewhere (11,12). However, CTL activity was not measured in the post-vaccination follow-up study primarily due to the limited number of available samples.

In previously reported HCV vaccine trials (9-13), as well as in the present follow-up study, there has yet to be a sustained

viral responder, regardless of the fact that successful immune responses have been induced in a substantial number of patients. The well-recognized difficulty of developing either prophylactic or therapeutic HCV vaccines largely results from viral heterogeneity and mutability (6-8). In addition, many studies have demonstrated suppressed or imbalanced immunity in CH or LC patients with HCV (25,26,30). Previous and present results, when taken together, suggest that developing an HCV vaccine to induce SVR as a primary endpoint will not be feasible until novel scientific breakthroughs in this field have been made. However, HCV peptide vaccines may augment both cellular and humoral responses against HCV-derived peptides in a large percentage of patients. This potential of peptide vaccines provides some hope that boosted specific immunity eliminates cancerous liver cells infected with HCV, which in turn may result in prevention or delay of HCC development associated with HCV. Indeed, the results of the present study support this hypothesis. Further clinical studies are required to confirm whether or not peptide vaccination using CTL epitopes derived from HCV protein are effective for prophylaxis against HCC in HCV-positive patients without SOL.

Acknowledgements

This study was supported in part by Grants-in-Aid from the Ministry of Education, Science, Sports and Culture of Japan to the Research Center of Innovative Cancer Therapy of the 21st Century Center of Excellence (COE) Program for Medical Science, and to Toshi-area Research.

References

1. World Health Organization (WHO) Hepatitis C. 2006. Available at: http://www.who.int/vaccine_research/diseases/viral_cancers/en/index2.html#disease%20burden
2. Chander G, Sulkowski MS, Jenckes MW, Torbenson MS, Herlong HF, Bass EB and Gebo KA: Treatment of chronic hepatitis C: a systematic review. Hepatology 36: S135-S144, 2002.
3. Kato N, Hijikata M, Ootsuyama Y, Nakagawa M, Ohkoshi S and Sugimura T: Molecular cloning of the human hepatitis C virus genome from Japanese patients with non-A, non-B hepatitis. Proc Natl Acad Sci USA 87: 9524-9528, 1990.
4. Blatt LM, Mutchnick MG, Tong MJ, *et al*: Assessment of hepatitis C virus RNA and genotype from 6807 patients with chronic hepatitis C in the United States. J Viral Hepat 7: 196-202, 2000.
5. Yoshida H, Shiratori Y, Moriyama M, *et al*: Interferon therapy reduces the risk for hepatocellular carcinoma: national surveillance program of cirrhotic and noncirrhotic patients with chronic hepatitis C in Japan. IHIT Study Group. Inhibition of Hepatocarcinogenesis by Interferon Therapy. Ann Intern Med 131: 174-181, 1999.
6. Houghton M and Abrignani S: Prospects for a vaccine against the hepatitis C virus. Nature 436: 961-966, 2005.
7. Strickland GT, El-Kamary SS, Klenerman P and Nicosia A: Hepatitis C vaccine: supply and demand. Lancet Infect Dis 8: 379-386, 2008.
8. Bowen DG and Walker CM: Mutational escape from CD8+ T cell immunity: HCV evolution, from chimpanzees to man. J Exp Med 201: 1709-1714, 2005.
9. Schlaphoff V, Klade CS, Jilma B, *et al*: Functional and phenotypic characterization of peptide-vaccine-induced HCV-specific CD8+ T cells in healthy individuals and chronic hepatitis C patients. Vaccine 25: 6793-6806, 2007.
10. Klade CS, Wedemeyer H, Berg T, *et al*: Therapeutic vaccination of chronic hepatitis C nonresponder patients with the peptide vaccine IC41. Gastroenterology 134: 1385-1395, 2008.
11. Yutani S, Yamada A, Yoshida K, *et al*: Phase I clinical study of a personalized peptide vaccination for patients infected with hepatitis C virus (HCV) 1b who failed to respond to interferon-based therapy. Vaccine 25: 7429-7435, 2007.
12. Yutani S, Komatsu N, Shichijo S, *et al*: Phase I clinical study of a peptide vaccination for hepatitis C virus-infected patients with different HLA-class I-A alleles. Cancer Science 100: 1935-1942, 2009.
13. Leroux-Roels G, Batens AH, Desombere I, *et al*: Immunogenicity and tolerability of intradermal administration of an HCV E1-based vaccine candidate in healthy volunteers and patients with resolved or ongoing chronic HCV infection. Hum Vaccin 1: 61-65, 2005.
14. Niu Y, Terasaki Y, Komatsu N, *et al*: Identification of peptides applicable as vaccines for HLA-A26-positive cancer patients. Cancer Science 100: 2167-2174, 2009.
15. Cerny A, McHutchison JG, Pasquinelli C, *et al*: Cytotoxic T lymphocyte response to hepatitis C virus-derived peptides containing the HLA A2.1 binding motif. J Clin Invest 95: 521-530, 1995.
16. Kiyosawa K, Umemura T, Ichijo T, *et al*: Hepatocellular carcinoma: recent trends in Japan. Gastroenterology 127: S17-S26, 2004.
17. Taura K, Ikai I, Hatano E, *et al*: Influence of coexisting cirrhosis on outcomes after partial hepatic resection for hepatocellular carcinoma fulfilling the Milan criteria: an analysis of 293 patients. Surgery 142: 685-694, 2007.
18. Shiratori Y, Shiina S, Teratani T, *et al*: Interferon therapy after tumor ablation improves prognosis in patients with hepatocellular carcinoma associated with hepatitis C virus. Ann Intern Med 138: 299-306, 2003.
19. Kubo M, Sakaguchi Y, Chung H, *et al*: Long-term interferon maintenance therapy improves survival in patients with HCV-related hepatocellular carcinoma after curative radiofrequency ablation. A matched case-control study. Oncology 72: 132-138, 2007.
20. Kim JH, Han KH, Lee KS, *et al*: Efficacy and long term follow up of combination therapy with interferon alpha and ribavirin for chronic hepatitis C in Korea. Yonsei Medical Journal 47: 793-798, 2006.
21. Arase Y, Ikeda K, Suzuki F, *et al*: Long term outcome after interferon therapy in elderly patients with chronic hepatitis C. Intervirology 50: 16-23, 2007.
22. Ikeda K, Saitoh S, Arase Y, *et al*: Effect of interferon therapy on hepatocellular carcinogenesis in patients with chronic hepatitis type C: a long-term observation study of 1,643 patients using statistical bias correction with proportional hazard analysis. Hepatology 29: 1124-1130, 1999.
23. Toyoda H, Kumada T, Tokuda A, *et al*: Long-term follow-up of sustained responders to interferon therapy in patients with chronic hepatitis C. J Viral Hepatitis 7: 414-419, 2007.
24. Okanoue T, Itoh Y, Minami M, *et al*: Interferon therapy lowers the rate of progression to hepatocellular carcinoma in chronic hepatitis C but not significantly in an advanced stage: a retrospective study in 1148 patients. J Hepatol 30: 643-649, 1999.
25. Bertoketti A, Bertoletti A, D'Elios MM, *et al*: Different cytokine profiles of intrahepatic T cells in chronic hepatitis B and hepatitis C virus infections. Gastroenterology 112: 193-199, 1997.
26. McGuinness PH, Painter D, Davies S and McCaughan GW: Increases in intrahepatic CD68 positive cells, MAC387 positive cells and proinflammatory cytokines (particularly interleukin 18) in chronic hepatitis C infection. Gut 46: 260-269, 2000.
27. Nelson DR, Lauwers GY, Lau JY and Davis GL: Interleukin 10 treatment reduces fibrosis in patients with chronic hepatitis C: a pilot trial of interferon nonresponders. Gastroenterology 118: 655-660, 2000.
28. Brière F, Servet-Delprat C, Bridon JM, Saint-Remy JM and Banchereau J: Human interleukin 10 induces naive surface immunoglobulin D+ (sIgD+) B cells to secrete IgG1 and IgG3. J Exp Med 179: 757-762, 1994.
29. Defrance T, Vanbervliet B, Brière F, *et al*: Interleukin 10 and transforming growth factor beta cooperate to induce anti-CD40-activated naive human B cells to secrete immunoglobulin A. J Exp Med 175: 671-682, 1992.
30. Rushbrook SM, Ward SM, Unitt E, *et al*: Regulatory T cells suppress in vitro proliferation of virus-specific CD8+ T cells during persistent hepatitis C virus infection. J Virol 79: 7852-7859, 2005.

Table 1 Selected differential disgnosis of fibrosing alopecia in a pattern distribution

Condition	Characteristics	Histology
Fibrosing alopecia in a pattern distribution	Alopecia in the distribution of typical male or female pattern hair loss Perifollicular erythema and hyperkeratosis	Miniaturization of hair follicles Lichenoid inflammatory infiltrate at isthmus and infundibular region perifollicular lamellar fibrosis
Androgenetic alopecia	Pattern baldness on the bitemporal areas and crown of the scalp	Miniaturized vellus follicles Increased telogen hairs in late stage
Frontal fibrosing alopecia	Cicatricial frontotemporal hair line recession Almost exclusively in postmenopausal women Perifollicular erythema and hyperkeratosis	Perifollicular fibrosis Lymphocytic infiltration at the isthmus and infundibulum
Follicular degeneration syndrome	Cicatricial alopecia of the central scalp and enlarges centrifugally	Premature inner root sheath desquamation Lymphocytic infiltration at the upper follicle Perifollicular concentric fibrosis
Pseudopelade of Brocq	Multiple round or irregularly shaped, hairless, cicatrial patches	Early stage: perifollicular lymphocytic infiltration Late stage: follicular longitudinal fibrous tract extended into subcutis

replacement of follicles with fibrosis in cicatricial alopecia. The striking differences between AGA/FPHL and FAPD include perifollicular erythema, perifollicular hyperkeratosis and loss of follicular orifices in the central scalp in FAPD.[1,3]

Cicatricial alopecia, including frontal fibrosing alopecia (FFP), follicular degeneration syndrome (FDS) and pseudopelade of Brocq share some clinical and histological evidence of the scarring process with FAPD.[1]

Frontal fibrosing alopecia is characterized with unique cicatricial frontotemporal hair line recession and almost exclusively presents in postmenopausal women.[5] Centrifugal and progressive hair loss starting at midscalp in our patient make the diagnosis of FFP less likely. Unlike FAPD, miniaturized hair follicles are rarely observed in FFP.

Pseudopelade of Brocq usually presents with multiple round, oval or irregularly shaped, hairless, cicatrial patches of varying sizes, which can distinguish it from FAPD.[5] Follicular erythema and hyperkeratosis are not typical features in pseudopelade of Brocq.

Follicular degeneration syndrome is a condition that presents with flesh-coloured, non-inflammatory cicatricial alopecia of the central scalp that, over time, enlarges centrifugally.[5] Histologically, the premature degeneration of the inner root sheath and migration of the hair shaft through the outer root sheath in the follicular degeneration are not seen in the histology of FAPD.[1,4]

Author contributions

Hsien-Yi Chiu: drafting of the manuscript, Sung-Jan Lin: case management and critical revision of the manuscript.

H-Y Chiu,† S-J Lin†,‡,*

†Department of Dermatology, National Taiwan University Hospital and National Taiwan University College of Medicine, Taipei, Taiwan, and ‡Institute of Biomedical Engineering, National Taiwan University, Taipei, Taiwan

*Correspondence: S-J Lin. E-mail: drsjlin@ntu.edu.tw

References

1 Zinkernagel MS, Trueb RM. Fibrosing alopecia in a pattern distribution: patterned lichen planopilaris or androgenetic alopecia with a lichenoid tissue reaction pattern? *Arch Dermatol* 2000; **136**: 205–211.
2 Kossard S. Postmenopausal frontal fibrosing alopecia. Scarring alopecia in a pattern distribution. *Arch Dermatol* 1994; **130**: 770–774.
3 Olsen EA. Female pattern hair loss and its relationship to permanent/cicatricial alopecia: a new perspective. *J Investig Dermatol Symp Proc* 2005; **10**: 217–221.
4 Sperling LC, Solomon AR, Whiting DA. A new look at scarring alopecia. *Arch Dermatol* 2000; **136**: 235–242.
5 Ross EK, Tan E, Shapiro J. Update on primary cicatricial alopecias. *J Am Acad Dermatol* 2005; **53**: 1–37; quiz 8–40.

DOI: 10.1111/j.1468-3083.2010.03580.x

Questionnaire-based survey of the treatment of patients with psoriasis and hepatitis C in Japan

Editor

Hepatitis C virus (HCV) is the most frequent aetiology of hepatitis in Japan, and a total of 1.5–2 million (1.2–1.5%) of Japanese are considered to be HCV positive. Combination therapy with pegylated interferon (IFN) alpha and ribavirin can eradicate approximately 80% of the HCV in chronic hepatitis C patients.[1] However, this therapy has various side-effects including the induction and/or exacerbation of psoriasis and psoriatic arthritis.[2–4] Therefore, HCV-positive patients with psoriasis encounter serious problems during treatment for their hepatitis.

Such patients also have problems in treating their psoriasis. Cyclosporine A (CyA), the most useful oral medication available

for psoriasis in Japan, was contraindicated for patients with chronic infections because of its strong immunosuppressive potential. However, recent research has revealed that CyA suppresses HCV replication *in vitro*[5,6] and *in vivo*.[7] We also previously reported a case of patients with psoriasis and hepatitis C successfully treated with CyA without worsening of their hepatitis.[8] To reach a consensus in treating HCV-positive patients with psoriasis, it is important to understand the current situation of the treatment modalities for such patients. Therefore, we carried out a questionnaire-based survey to estimate the frequency of HCV-positive patients with psoriasis in Japan and how they are treated.

A questionnaire asking the number of the patients with psoriasis and hepatitis C, and the dermatological and hepatological therapies was sent to dermatologists who were all members of the Japanese Dermatological Association (JDA).

A total of 234 completed questionnaires (38.9%) were returned (Table 1). Overall, 38% (88/234) of the dermatologists were treating HCV-positive patients with psoriasis.

The dermatologists in the university hospitals treated HCV-positive psoriasis patients more frequently (52%, 61/118) than the dermatologists in community hospitals (30%, 17/56) and practitioners (18%, 11/60). On average, the dermatologists treated 1.25 HCV-positive psoriasis patients at university hospitals, 0.46 patients at community hospitals and 0.44 patients at clinics (overall average of 0.85 patients per dermatologist).

Dermatologists employed topical corticosteroid and topical vitamin D3 cream most frequently followed by phototherapy, and CyA was used by 24% of dermatologists (Fig. 1a).

On treating hepatitis C, glycyrrhizin or ursodeoxycholic acid was administered by 45% of the internists, while IFN alpha was chosen by 40% of the internists and maximum of 99 patients underwent IFN therapy. In 28% of the patients, the dermatologists were not aware of the hepatitis therapy their patients were undergoing (Fig. 1b).

Our results showed that 38% of dermatologists in Japan treated HCV-positive patients with psoriasis, providing an average of 0.85 such patients per dermatologist. Based on the total number of dermatologists in Japan, approximately 7000 HCV-positive psoriasis patients may reside in Japan. Dermatologists in HCV-thriving countries should be aware of how their patients are treated by internists.

In addition to topical therapies, 24% of the dermatologists used CyA to treat psoriasis in patients with hepatitis C. This finding reveals that dermatologists no longer consider CyA to be a contraindication for patients with hepatitis C. CyA is providing more preferable therapeutic results in HCV-positive recipients in liver

Table 1 Results for the returned questionnaires

Facilities	Sent	Returned	Return ratio (%)	No. dermatologists with a positive response	Positive ratio (%)	No. patients	Mean patient number per dermatologist
University hospitals	309	118	38.2	61	51.7	147	1.25
Community hospitals	128	56	43.8	17	30.4	30	0.54
Dermatology clinics	159	60	37.7	11	18.3	26	0.43
Total	596	234	39.3	89	38.0	198	0.85

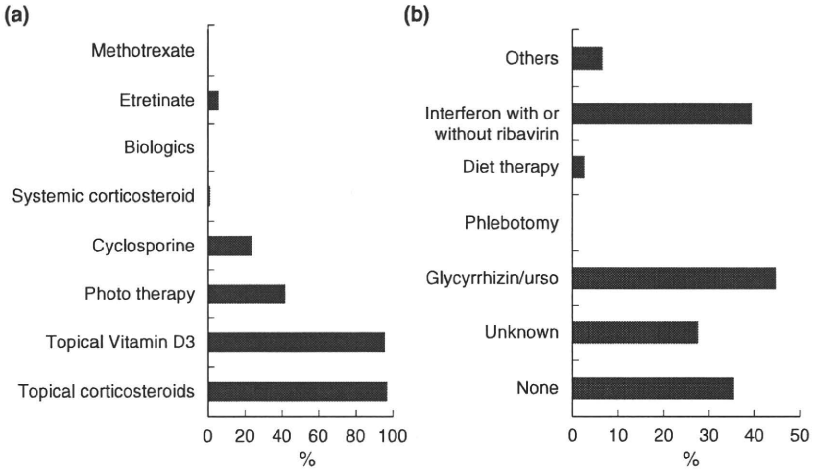

Figure 1 Treatment choices of (a) dermatologists and (b) internists for the treatment of patients with psoriasis and hepatitis C. Urso, ursodeoxycholic acid.

transplantation[9] and HCV-positive patients with autoimmune diseases.[10]

Regarding the treatments for hepatitis employed by internists, it was a surprising finding that 40% of institutions employed IFN alpha therapy for patients with psoriasis. We plan to further examine the detailed information for these patients.

Twenty-eight per cent of dermatologists answered that they were not aware of the hepatitis therapies employed by the internists. As administration of IFN alpha has a risk of exacerbating psoriasis, dermatologists should know the way in which their patients are being treated by internists, and informed consent should be obtained from the patients before IFN alpha treatment.

Acknowledgements

This study was supported in part by Health and Labour Sciences Research Grants for Research on Hepatitis from the Ministry of Health, Labour and Welfare of Japan.

S Imafuku,* J Nakayama

Department of Dermatology, Faculty of Medicine, Fukuoka University, Fukuoka, Japan

*Correspondence: S Imafuku. E-mail: dermatologist@mac.com

References

1 Ide T, Hino T, Ogata K *et al.* A randomized study of extended treatment with peginterferon alpha-2b plus ribavirin based on time to HCV RNA negative-status in patients with genotype 1b chronic hepatitis C. *Am J Gastroenterol* 2009; **104**: 70–75.

2 Quesada JR, Gutterman JU. Psoriasis and alpha-interferon. *Lancet* 1986; **1**: 1466–1468.

3 Jucgla A, Marcoval J, Curco N, Servitje O. Psoriasis with articular involvement induced by interferon alfa. *Arch Dermatol* 1991; **127**: 910–911.

4 Gota C, Calabrese L. Induction of clinical autoimmune disease by therapeutic interferon-alpha. *Autoimmunity* 2003; **36**: 511–518.

5 Watashi K, Hijikata M, Hosaka M *et al.* Cyclosporin A suppresses replication of hepatitis C virus genome in cultured hepatocytes. *Hepatology* 2003; **38**: 1282–1288.

6 Watashi K, Ishii N, Hijikata M *et al.* Cyclophilin B is a functional regulator of hepatitis C virus RNA polymerase. *Mol Cell* 2005; **19**: 111–122.

7 Inoue K, Sekiyama K, Yamada M *et al.* Combined interferon alpha2b and cyclosporin A in the treatment of chronic hepatitis C: controlled trial. *J Gastroenterol* 2003; **38**: 567–572.

8 Imafuku S, Tashiro A, Furue M. Ciclosporin treatment of psoriasis in a patient with chronic hepatitis C. *Br J Dermatol* 2007; **156**: 1367–1369.

9 Cescon M, Grazi GL, Cucchetti A *et al.* Predictors of sustained virological response after antiviral treatment for hepatitis C recurrence following liver transplantation. *Liver Transpl* 2009; **15**: 782–789.

10 Manna R, Verrecchia E, Fonnesu C *et al.* Cyclosporine A: good response for patients affected by autoimmune disorders and HCV infection? *Eur Rev Med Pharmacol Sci* 2009; **1**: 63–69.

DOI: 10.1111/j.1468-3083.2010.03586.x

A missense mutation in KRT14 causing a dermatopathia pigmentosa reticularis/Naegeli–Franceschetti–Jadassohn phenotype

Editor

Naegeli–Franceschetti–Jadassohn syndrome and dermatopathia pigmentosa reticularis (NFJS/DPR) are highly similar disorders characterized by core symptoms of reticular hyperpigmentation of the skin, palmoplantar keratoderma, nail dystrophy and reduced sweating. Various associated abnormalities include blistering, poor teeth, reduced or absent dermatoglyphics and hypotrichosis. In 2006, Lugassy *et al.* found heterozygous non-sense and frameshift mutations in the E1 and V1 domains of keratin 14 (KRT14) in five families with DPR/NFJS;[1] as a consequence, the two disorders are now considered allelic. All mutations were predicted to result in early termination of translation and it was speculated that KRT14 plays a role in early development of the epidermis and its appendages. The N-terminus has been shown to confer protection against apoptosis and increased apoptotic activity was indeed shown in the basal layer of patient epidermis.[2] The origin of the hyperpigmentation is less clear, but might relate to melanosome trafficking. Alternatively, pigmentary incontinence secondary to basal keratinocyte apoptosis might be responsible. Lugassy *et al.* have speculated that the NFJS/DPR mutations do not result in non-sense-mediated mRNA decay, but do allow for the production of a truncated KRT14 protein which then exerts a dominant negative effect. In support of their hypothesis, autosomal recessive EBS can be caused by truncating mutations affecting more distal domains of the protein.[3] However, formal proof for this hypothesis is lacking and finding a NFJS/DPR phenotype associated with more distal or missense mutations would put it in doubt. Here, we describe a patient with a DPR/NFJS phenotype caused by a missense mutation in KRT14.

The patient is a 41-year-old woman of Dutch descent who was referred to our outpatient clinic for flexural hyperpigmentation that had been present for as long as she could recall, but had been more pronounced when she was younger. She had never experienced blistering and did not complain of reduced sweating. Her nails did not grow well, but broke easily. The patient was otherwise healthy. There were no affected family members and she had no children. Upon physical examination, there was reticulate hyperpigmentation in both axillae, the neck and bilaterally in the inguinal region (Fig. 1a). Some mottled pigmentation was also visible on the dorsa of the fingers. The fingertips had reduced dermatoglyphics and there was clear nail dystrophy (Fig. 1b,c). Hair and teeth were normal. Blistering was absent. Based on the nail dystrophy, reduced dermatoglyphics and reticulate

Chronic Hepatitis and Cirrhosis on MR Imaging

Tatsuyuki Tonan, MD[a], Kiminori Fujimoto, MD, PhD[a,b], Aliya Qayyum, MD, MRCP, FRCR[c,*]

KEYWORDS

- Liver cirrhosis • Hepatitis
- Liver-specific MR contrast agent • Fibrosis
- Regenerative nodule • Dysplastic nodule
- Well-differentiated hepatocellular carcinoma

Chronic liver diseases represent a major cause of morbidity and mortality worldwide. The major origins of chronic liver disease and also leading causes of cirrhosis and hepatocellular carcinoma (HCC) are chronic infection with hepatitis B virus (HBV) and hepatitis C virus (HCV), and alcoholic and nonalcoholic fatty liver disease. Magnetic resonance (MR) imaging has been increasingly used to evaluate diffuse parenchymal abnormalities of the liver. Morphologic changes and signal intensity effects not only facilitate the diagnosis of chronic liver disease with MR imaging, but may help to distinguish between differing etiology and assist in staging severity. Moreover, recent advances in the development of MR systems and liver-specific MR contrast agents such as superparamagnetic iron oxide (SPIO) and gadoxetic acid (Gd-EOB-DTPA) have expanded the potential utility of MR imaging in the accurate depiction of specific disorders and cirrhosis-associated hepatocellular nodules.

In this article, the authors focus on the current role of MR imaging in the detection and characterization of chronic hepatitis and cirrhosis. In particular, the characteristic MR imaging features of morphologic changes and focal manifestations of chronic liver disease are highlighted.

DEFINITION, ETIOLOGY, AND PREVALENCE

Chronic hepatitis is defined as a continuous or recurrent inflammation of the liver for more than 6 months, with histologic changes of chronic liver damage. Pathologically it is characterized by lymphocytic infiltration, liver cell injury, necrosis, and fibrosis.[1] Chronic hepatitis progresses from mild inflammation, to more severe inflammation and fibrosis, and eventually to cirrhosis. Cirrhosis is characterized by the replacement of liver tissue by fibrosis, scar tissue, and regenerative nodules, leading to the deterioration of liver function.[2]

The most common causes of cirrhosis in the United States[3] are HBV and HCV infection, either singly or combined, and alcohol abuse. Other causes of cirrhosis include nonalcoholic fatty liver disease, hemochromatosis, autoimmune disease, Wilson disease, primary sclerosing cholangitis, and primary biliary cirrhosis.

The clinical importance of chronic liver disease is reflected in the large numbers of affected patients and the frequency of the associated serious complications. Approximately 400 million people are chronically infected with HBV worldwide,[4] of whom 25% to 40% die of cirrhosis and its end-stage complications. Chronic hepatitis C further affects approximately 200 million people

[a] Department of Radiology, Kurume University School of Medicine, 67 Asahi-machi, Kurume 830-0011, Japan
[b] Department of Radiology, Center for Diagnostic Imaging, Kurume University Hospital, 67 Asahi-machi, Kurume 830-0011, Japan
[c] Department of Radiology and Biomedical Imaging, University of California San Francisco, 505 Parnassus Avenue, Room L-307, Box 0628, San Francisco, CA 94143, USA
* Corresponding author.
E-mail address: aliya.qayyum@radiology.ucsf.edu

Magn Reson Imaging Clin N Am 18 (2010) 383–402
doi:10.1016/j.mric.2010.08.011
1064-9689/10/$ – see front matter

with a greater prevalence in Western countries.[5] The development of cirrhosis is common in chronic HCV, and the risk of HCC is 3% to 4% per year.[6] Once chronic HCV infection is established, cirrhosis develops within 10 to 20 years in approximately 20% of patients.[7] An estimated 10,000 deaths annually have been attributed to HCV-related diseases, and it is suggested that HCV may be responsible for nearly half of all HCC cases.

Alcoholic liver disease is among the most important causes of morbidity and mortality in the United States, accounting for up to 12,000 deaths each year, and representing more than 50% of liver disease–related deaths.[8,9] Nonalcoholic fatty liver disease (NAFLD) is now recognized as an important clinical entity, affecting approximately 20% to 30% of the adult population in the Western world.[10] NAFLD represents a disease spectrum ranging from isolated steatosis to more advanced disease with necroinflammatory change and fibrosis (nonalcoholic steatohepatitis or NASH), to cirrhosis in its most severe form. The prevalence of obesity and NAFLD in the United States translates into a substantial clinical problem, with more than 19% of obese individuals and 2% to 3% of the general population presenting with NASH.[10]

MR IMAGING FEATURES

Morphologic and Signal Intensity Changes

Hepatitis is associated with infiltration of inflammatory cells in to the liver, which results in liver cell injury and edema. Such liver changes may be visualized as periportal edema, which is characterized by high signal intensity bands paralleling the portal vessels on T2-weighted images (**Fig. 1**).

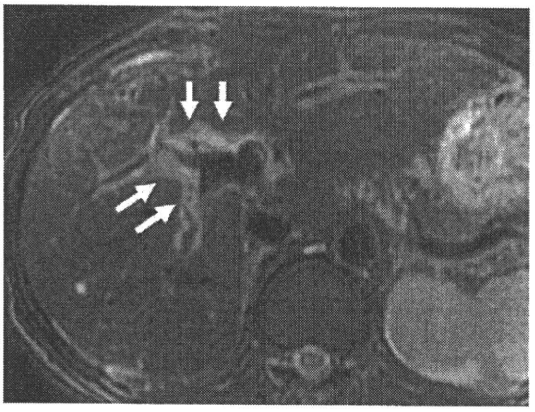

Fig. 1. T2-weighted fat-saturated turbo spin-echo (TSE) image (repetition time/echo time [TR/TE] = 4600/99 ms) in a patient with chronic hepatitis due to autoimmune hepatitis shows regions of high signal intensity bands paralleling the portal vessels (*arrow*).

Periportal edema is a common but nonspecific imaging finding in patients with severe acute hepatitis[11] and is also described in chronic viral hepatitis.[1] A similar appearance may also be seen in patients with malignant lymphadenopathy in the porta hepatis, biliary obstruction, cirrhosis, hepatic trauma, or transplant rejection.[12]

As cirrhosis progresses from early to advanced or end stage, it gives rise to several intra- and extrahepatic changes, including regional morphologic changes in the liver, nodularity of the liver surface, splenomegaly, regenerative nodules, iron and fat deposition, and ascites, and the development of varices and collaterals.[13] Although the classically described findings of cirrhosis are common in advanced cirrhosis, they are seen less frequently in the early stage of the disease, at which time the liver may appear normal on cross-sectional imaging, occasionally hampering imaging-based diagnosis.[14]

Enlargement of the hilar periportal space[14] (**Fig. 2**) on MR imaging has been shown to be a useful sign in the diagnosis of early cirrhosis. It has been reported that this sign is visible in 98% of patients with early cirrhosis who do not have conventional signs (ie, splenomegaly, portosystemic collateral vessels, ascites, or surface nodularity), whereas this sign is seen in only 11% of patients with normal livers.[15] Often, expansion of the major interlobar fissure[16] (see **Fig. 2**) is seen in these patients with early cirrhosis. These findings are attributed to atrophy of the medial segment of the left hepatic lobe, suggesting that medial segment atrophy may be an initial morphologic change in early cirrhosis.[17]

Hepatic morphologic changes typically seen in advanced cirrhosis include hypertrophy of the caudate lobe and lateral segments of the left lobe, and atrophy of both posterior segments of the right lobe and the medial segment of the left lobe.[17] Other morphologic changes with high specificity for a diagnosis of cirrhosis include the expanded gallbladder fossa sign (**Fig. 3**),[18] which is defined as enlargement of the pericholecystic space (ie, gallbladder fossa), and the right posterior hepatic notch sign (see **Fig. 3**),[19] which is defined as a sharp indentation in the right medial posterior surface of the liver (**Table 1**).

The patterns of hepatic morphologic and signal intensity changes overlap among the different causes of cirrhosis. However, certain imaging features may suggest particular etiological factors, such as enlargement of the lateral segment accompanied by shrinkage of both the right lobe and left medial segment, which reportedly frequently occurs in patients with viral-induced cirrhosis. Conversely, previous study showed

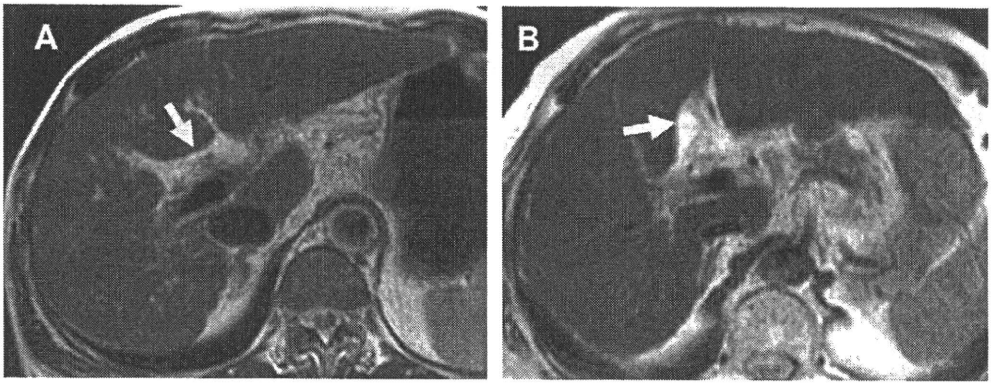

Fig. 2. T2-weighted TSE image in early cirrhosis shows enlargement of the hilar periportal space between the left medial segment and the right portal vein (*A*) (*arrow*) and expansion of the major interlobar fissure (*B*) (*arrow*) between the left medial and lateral segments.

that the mean values of the volume index of the caudate lobe were significantly greater in patients with alcoholic cirrhosis than in patients with viral cirrhosis.[20] Marked caudate lobe enlargement is typically associated with alcoholic cirrhosis.[20]

Primary sclerosing cholangitis (PSC) and primary biliary cirrhosis (PBC) have several distinctive features that may help to differentiate them from other types of cirrhosis (**Table 2**). PSC is reportedly associated with hypertrophy of the caudate lobe and atrophy of the other areas (medial segment, lateral segment, and right hepatic lobe, either individually or in combination) (**Fig. 4**).[21] Previous study showed that these findings were observed in 68% (ie, hypertrophy of the caudate lobe) and 55% (ie, atrophy of the other areas) of patients with PSC, respectively.[21] Other etiologies, such as Budd-Chiari syndrome also demonstrate hypertrophy of the caudate lobe and variable atrophy/hypertrophy of the remaining portions of the liver.[22] In addition, irregular intra- and/or extrahepatic bile duct dilatation and stenosis are also observed. The arterial or delayed phase of contrast-enhanced dynamic MR imaging demonstrates increased enhancement of the hepatic parenchyma surrounding the dilated

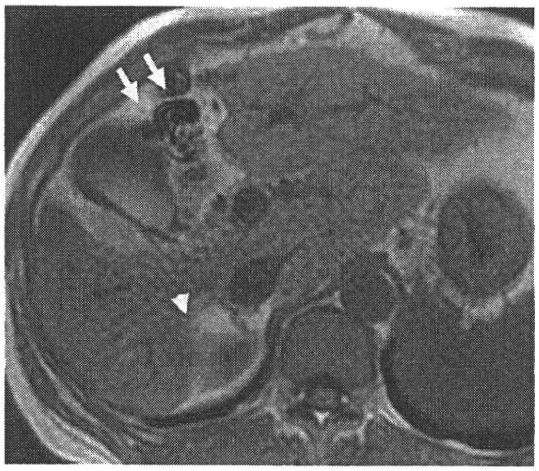

Fig. 3. T1-weighted gradient-echo (GRE) in-phase (TE, 4.7 ms) image in advanced cirrhosis shows enlargement of the pericholecystic space, presenting the expanded gallbladder fossa sign (*arrows*), and sharp indentation in the right medial posterior surface, presenting the right posterior hepatic notch sign (*arrowhead*).

Table 1
Typical morphologic changes of liver cirrhosis

Early Cirrhosis	Advanced Cirrhosis
Enlargement of the hilar periportal space	Hypertrophy of caudate lobe and/or lateral segments
Expansion of the major interlobar fissure	Atrophy of medial and/or posterior segments
	Enlargement of the pericholecystic space (expanded gallbladder fossa sign)
	Hepatic sharp indentation in the posterior surface (right posterior hepatic notch sign)

Data from Refs.[12–16]

Table 2
Distinctive morphologic changes and appearance of PSC and PBC at MR imaging

	Morphologic Changes	Appearance on MR Imaging
PSC	Hypertrophy of caudate lobe Atrophy of medial segment, lateral segment, right hepatic lobe (or all of 3 segments) Dilatation and stenosis of intra- and/or extrahepatic bile duct	Dynamic MR imaging[a] Increased enhancement of local hepatic parenchyma SPIO[b] Decreased enhancement of local hepatic parenchyma Gd-EOB-DTPA[c] Decreased enhancement of local hepatic parenchyma
PBC	Nonspecific	Periportal hyperintensity (hyperintense on T2WI) MR imaging periportal halo sign (hypointense on T1WI and T2WI)

Abbreviations: PBC, primary biliary cirrhosis; PSC, primary sclerosing cholangitis; WI, weighted imaging.
[a] T1-weighted GRE image on arterial- and portal phase after administration of gadolinium-based contrast agents.
[b] T2-weighted GRE image after administration of superparamagnetic iron oxide (SPIO).
[c] T1-weighted GRE image on hepatocyte-selective phase after administration of gadoxetic acid (Gd-EOB-DTPA).
Data from Refs.[17–19]

intrahepatic bile duct (**Fig. 5**), which is considered to represent fibrotic changes and hepatocyte damage.[21] In the authors' experience, the periductal parenchyma in PSC does not show uptake of SPIO, a liver-specific MR contrast agent normally taken up by hepatic Kupffer cells (**Fig. 6**). A reduced uptake of hepatobiliary-specific contrast agents (ie, Gd-EOB-DTPA, discussed later) is also observed (see **Fig. 6**).

MR findings that have been shown to be helpful in the diagnosis of PBC include periportal hyperintensity on T2-weighted images and the periportal halo sign (**Fig. 7**). Periportal hyperintensity on T2-weighted MR images has been attributed to periportal inflammation.[23] One study reported that periportal hyperintensity (see **Fig. 7**) was observed in 100% of patients with PBC with histologic stage I or II disease, 75% of patients with stage III disease, and 33% of patients with stage IV disease.[24] Forty-three percent of patients with PBC are reported to demonstrate the periportal halo sign (see **Fig. 7**), which is depicted as periportal signal hypointensity on T1- and T2-weighted

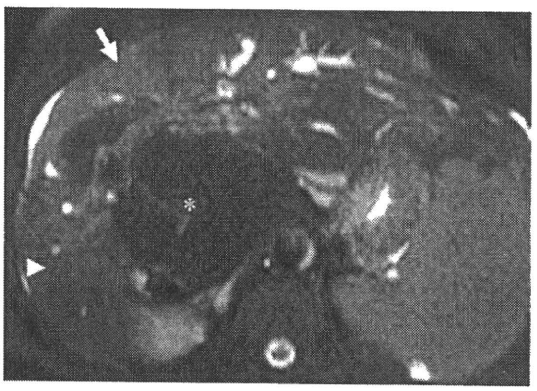

Fig. 4. T2-weighted fat-saturated TSE image in a patient with primary sclerosing cholangitis (PSC) shows hypertrophy of the caudate lobe (*asterisk*), and atrophy of the medial segment (*arrow*) and right hepatic lobe (*arrowhead*).

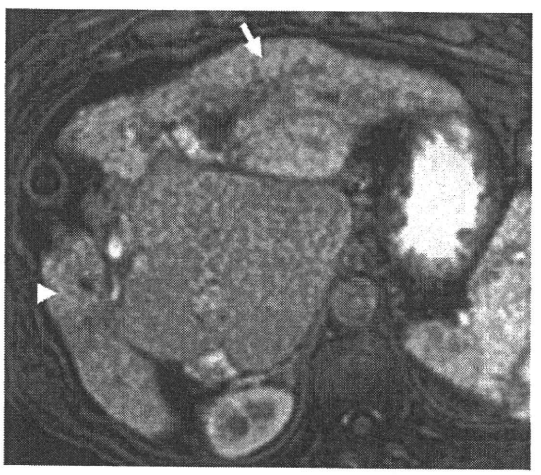

Fig. 5. Arterial-phase contrast-enhanced dynamic MR imaging shows slight increased enhancement of liver parenchyma in the lateral segment (*arrowhead*) and right hepatic lobe (*arrow*), which corresponds to the distribution of intrahepatic bile duct dilatation in comparison with that in caudate lobe. (Same patient as in **Fig. 4**.)

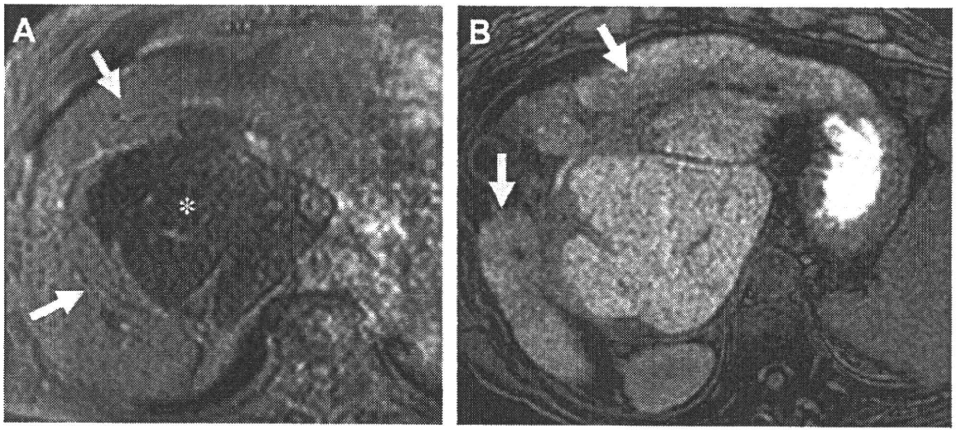

Fig. 6. T2-weighted GRE image (TE, 9.5 ms) within 10 minutes after administration of SPIO (*A*) demonstrates a high-intensity area in which SPIO particles are not taken up, presenting fibrotic change and hepatocyte damage (*arrows*). Conversely, uptake of SPIO particles is observed in the caudate lobe (*asterisk*). T1-weighted fat-saturated 3-dimensional (3D) gradient-echo (GRE) images (TR/TE = 3.6/1.7 ms, flip angle = 15°) in hepatocyte-selective phase (*B*) shows also decrease of uptake of Gd-EOB-DTPA (*arrows*). (Same patient as in **Fig. 4.**)

MR images.[23] It has been suggested that the MR imaging periportal halo sign may represent stellate, periportal, hepatocellular parenchymal extinction encircled by a rosette of large regenerating nodules.[23]

Portal Hypertension

In the cirrhotic liver, progressive hepatic fibrosis leads to increased vascular resistance at the level of the hepatic sinusoids, which results in a reduced portal contribution to liver perfusion.[25] The subsequent development of portal hypertension gives rise to complications such as ascites and the development of collateral vessels at the lower end of the esophagus (**Fig. 8**).[26] Portosystemic shunts also form through reopened paraumbilical veins (see **Fig. 8**) and the left gastric vein, which both normally drain into the portal vein.

The decreased portal venous supply that occurs as a result of liver fibrosis is partially compensated by an increase in arterial blood supply.[27] Such an increase in arterial perfusion may be demonstrated by pronounced liver enhancement in the first seconds after administration of intravenous contrast media in cirrhotic patients. Early patchy enhancement of liver parenchyma on MR imaging is a feature of portal hypertension, and is

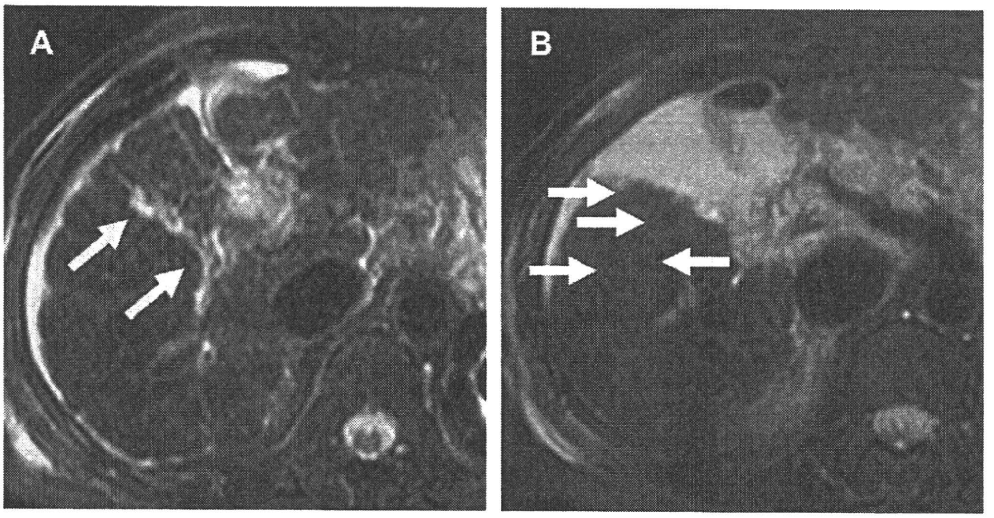

Fig. 7. T2-weighted fat-saturated TSE image in a patient with primary biliary cirrhosis shows periportal hyperintensity (*A*) (*arrows*) around portal tracts and around areas of low-intensity signal (*B*) (*arrows*) encircling the portal veins, presenting the periportal halo sign.

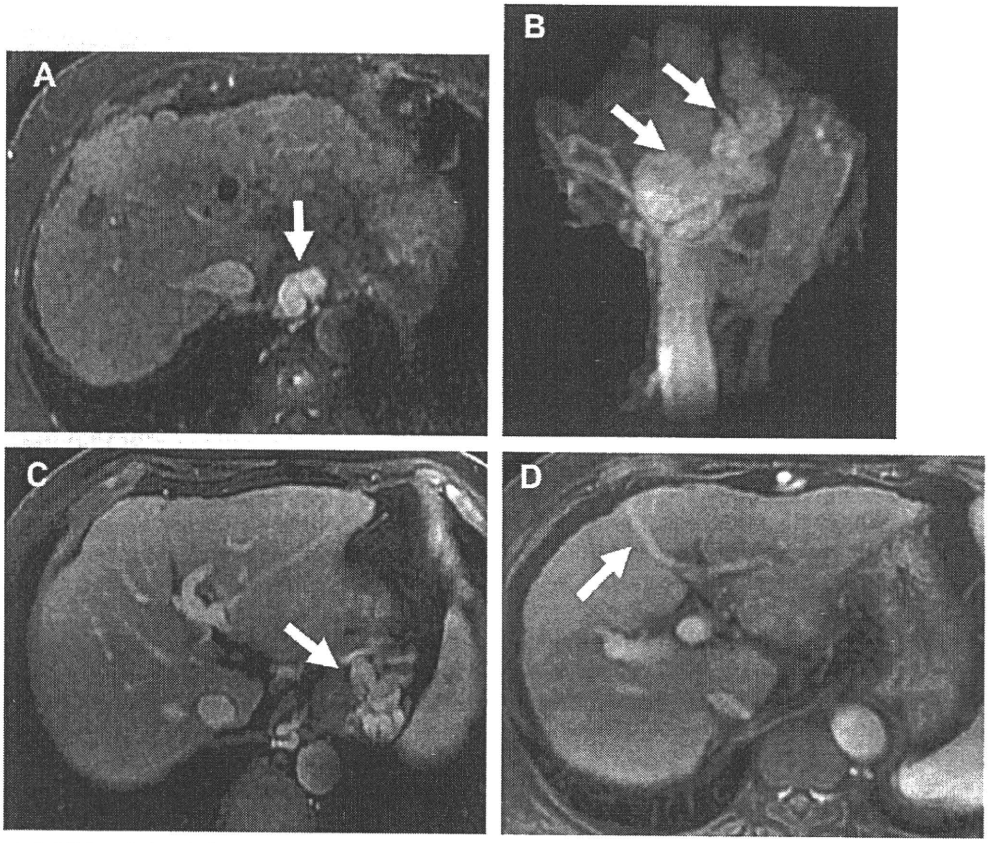

Fig. 8. Axial T1-weighted fat-saturated 3D GRE images (TR/TE = 3.3/1.5 ms, flip angle = 12°) (*A*, *C*, *D*) and maximum-intensity projection image (*B*) in portal phase after administration of Gd-EOB-DTPA at 3-T units shows examples of collateral vessel development in end-stage cirrhosis; dilated and tortuous esophageal varices (*A*, *B*) (*arrows*), gastric varices (*C*) (*arrow*), and recanalized paraumbilical veins (*D*) (*arrow*).

reportedly associated with the presence of numerous infiltrating macrophages, necrosis, tissue collapse, and increased steatosis (**Fig. 9**).[28]

Fibrosis

Pathologic characteristics and MR imaging features of liver fibrosis

Fibrosis is an inherent component of cirrhosis, and has MR imaging characteristics. In viral hepatitis, liver fibrosis begins and manifests as fibrous expansion of the portal triads (**Fig. 10**). Fibrous septa then grow from the expanded portal triad into the surrounding hepatic parenchyma. Subsequently, the fibrous septa lengthen and thicken to eventually form fibrous bridges that link adjacent portal triads and central veins (see **Fig. 10**). As the liver injury continues, the bridges continue to enlarge and coalesce and eventually divide the liver into rounded islands of hepatic parenchyma (regenerative nodules) surrounded by fibrosis tissue (see **Fig. 10**).[29] The pattern of early fibrosis

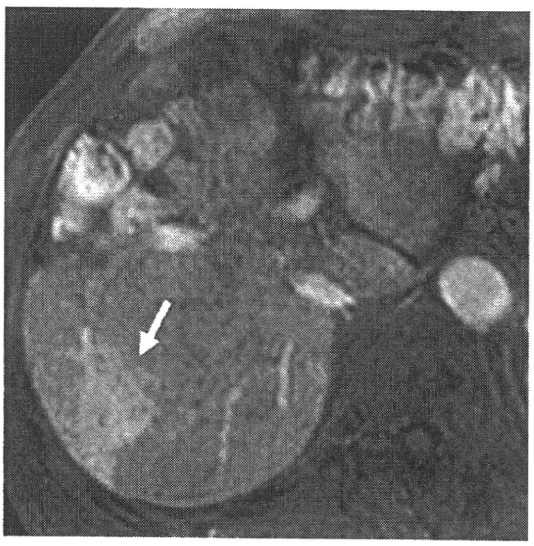

Fig. 9. Arterial-phase contrast-enhanced dynamic MR image shows increased enhancement of liver parenchyma (*arrow*), presenting early patchy enhancement.

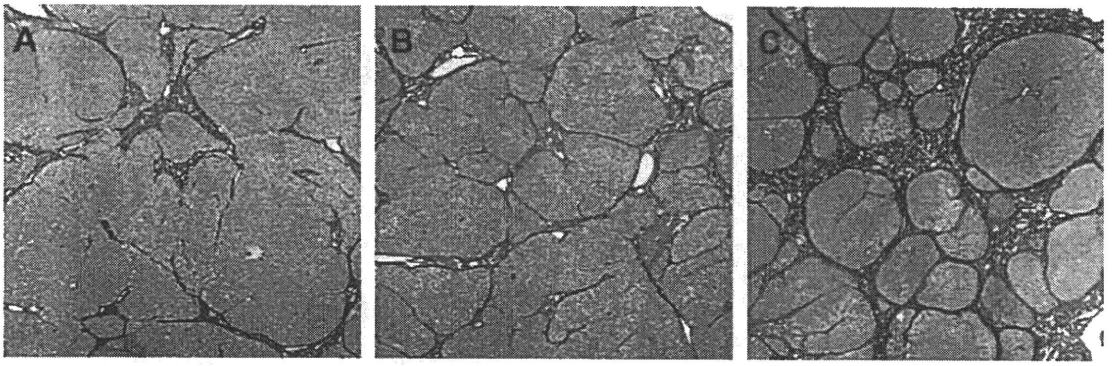

Fig. 10. Photomicrographs (Azan-Mallory stain, original magnification ×20) in a patient with hepatitis C virus infection (HCV) shows chronic hepatitis (*A*), early cirrhosis (*B*), and advanced cirrhosis (*C*). *A* shows moderate fibrosis without lobular distortion, and *B* shows advanced fibrosis having a tendency of lobular distortion. *C* shows multiple regenerative nodules and wider fibrous septa surrounding these nodules. (*Courtesy of* Osamu Nakashima, MD, Department of Pathology, Kurume University School of Medicine, Japan.)

differs in alcoholic hepatitis and nonalcoholic fatty liver disease because early fibrosis first develops adjacent to the central veins rather than in the portal triads, but progressive fibrosis eventually shows the same pathologic findings as cirrhosis caused by viral hepatitis.[29,30]

The current reference examination in the assessment of liver fibrosis is liver biopsy. However, this procedure is invasive with recognized morbidity and mortality, and repeated biopsy for the monitoring of disease progression is accordingly suboptimal. In addition, the accuracy of biopsy remains controversial because of sampling variability caused by the small size of hepatic samples and the heterogeneity of liver fibrosis.[31] These limitations have stimulated the search for noninvasive approaches to the assessment of liver fibrosis.

Conventional MR imaging techniques and fibrosis

The MR imaging appearance of the fibrotic septa and bridges comprises reticulations surrounding regenerative nodules giving rise to the so-called lacelike pattern. The fibrous septa appear hypointense on T1-weighted images and hyperintense on T2-weighted images (**Fig. 11**),[16] which in part is attributed to large water content.[22]

Most gadolinium-based contrast agent formulations freely equilibrate with extracellular volumes, such as liver fibrosis, and thereby improve the visibility of fibrosis on MR imaging.[32] MR images obtained at the equilibrium and delayed phase after gadolinium administration show fibrotic septa and bridges as linear and reticulation enhancement patterns.[28] These findings are more prominent in the periphery of the liver.

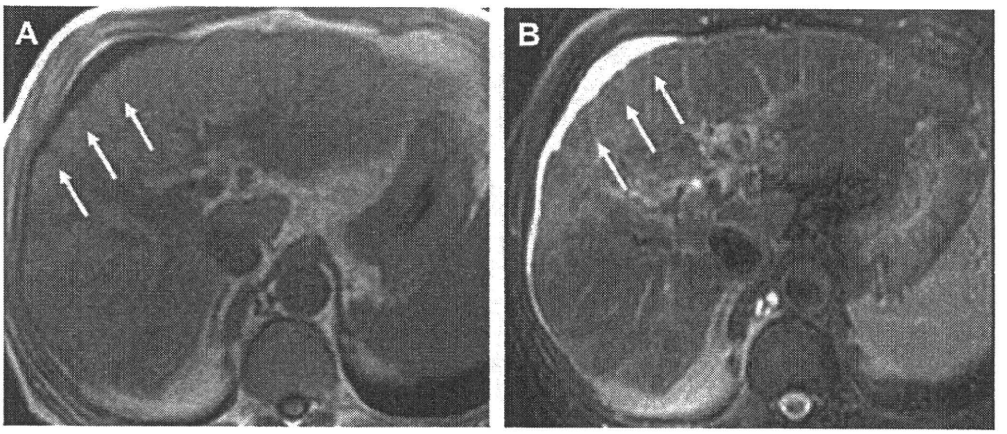

Fig. 11. T1-weighted GRE in-phase (TE, 4.7 ms) image and T2-weighted fat-saturated TSE image shows fibrotic septa and bridges as reticulations. The reticulations (*arrows*) are observed as hypointense on T1-weighted images (*A*) and as hyperintense on T2-weighted images (*B*).

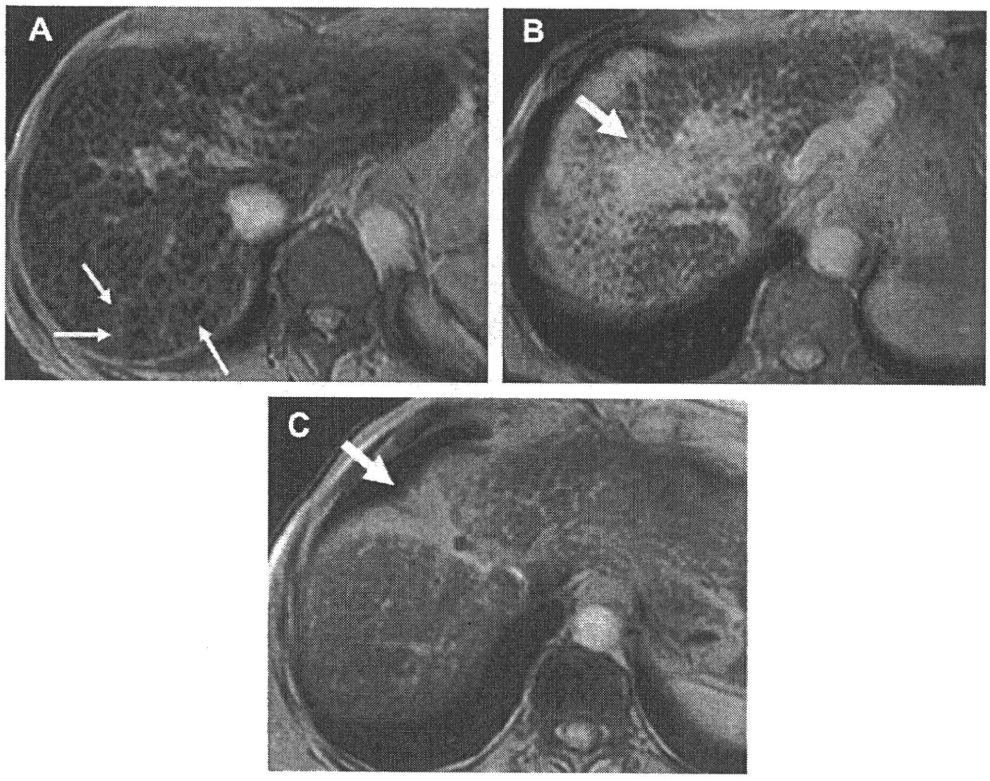

Fig. 12. T2-weighted GRE image (TE, 9.5 ms) after administration of SPIO distinctly demonstrates high-intensity reticulations (*A*) (*arrows*) and confluent fibrosis (*B* = wedge shape, *C* = geographic shape) (*arrow*), which do not take up SPIO particles in cirrhotic liver with HCV.

In end-stage liver cirrhosis, focal confluent fibrosis, which typically has a wedge shape or geographic shape with straight or concave borders, is occasionally observed in the subcapsular region.[22,29] The signal intensity and enhancement features of confluent fibrosis following administration of extracellular contrast agents are similar to those of fibrotic septa and bridges.

Liver-specific contrast agents and fibrosis

SPIO-enhanced MR imaging has been shown to be helpful in the detection of macroscopic fibrous bands and diffuse liver fibrosis. On T2-weighted turbo spin-echo and T2-weighted GRE images after administration of SPIO, the areas of fibrosis within the liver, which have reduced Kupffer cell density, accumulate less iron oxide

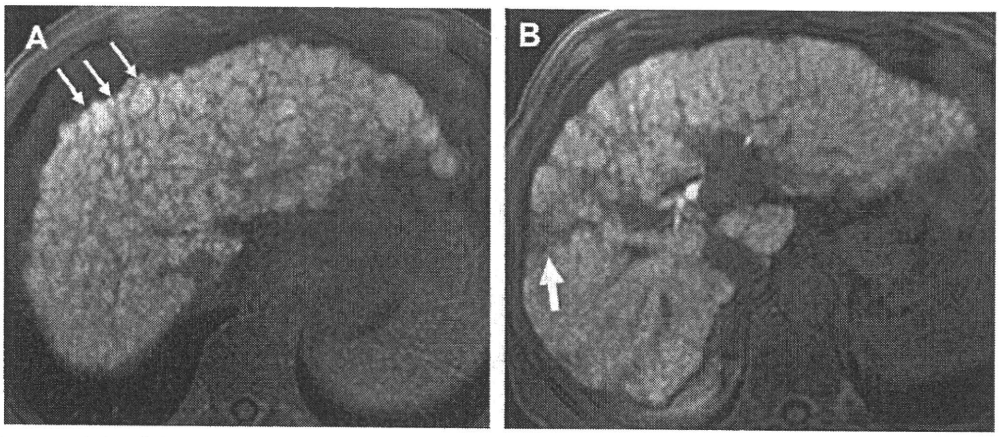

Fig. 13. T1-weighted fat-saturated 3D GRE image (TR/TE = 3.6/1.7 ms, flip angle = 15°) after administration of Gd-EOB-DTPA at hepatocyte-selective phases also clearly demonstrates fibrotic reticulations (*A*) and confluent fibrosis (*B* = wedge shape) (*arrows*).

Table 3
Macroscopic architectures and typical appearance of liver fibrosis at MR imaging

Macroscopic Findings	MR Imaging Form	Signal Intensity	Dynamic MR Imaging[a]	SPIO[b]	Gd-EOB-DTPA[c]
Fibrotic septa and bridge	Reticulation (lacelike pattern)	Hypointense (T1WI)	Increased enhancement	Hyperintense[d]	Hypointense[d]
Confluent fibrosis	Wedge shape or geographic shape	Hyperintense (T2WI)			

Abbreviations: Gd-EOB-DTPA, gadoxetic acid; SPIO, superparamagnetic iron oxide.
[a] T1-weighted GRE image on delayed phase after administration of gadolinium-based contrast agents.
[b] T2-weighted GRE image after administration of SPIO.
[c] T1-weighted GRE image on hepatocyte-selective phase after administration of Gd-EOB-DTPA.
[d] Appearance is described in comparison with the surrounding hepatic parenchyma.
Data from Refs.[13,23,24,26–28,30,31]

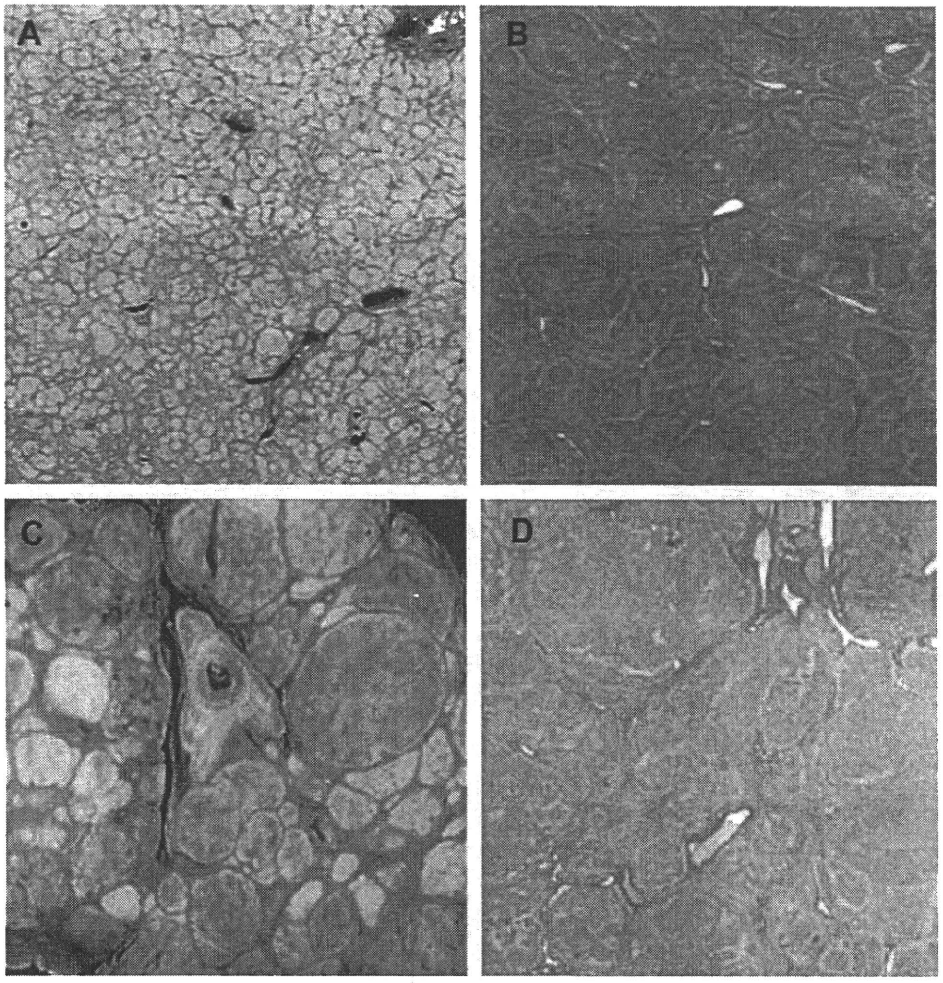

Fig. 14. Cirrhosis of micro- (*A*, *B*) and macronodular type (*C*, *D*). Gross appearance (*A*) and photomicrographs (Azan-Mallory stain, original magnification ×20) (*B*) show regenerative nodules (2–3 mm in size) with irregular shape in a case of cirrhotic liver with HCV. Gross appearance (*C*) and photomicrographs (Azan-Mallory stain, original magnification ×20) (*D*) show regenerative nodules (1–2 cm in size) with regular shape in a case of cirrhotic liver with HBV. (*Courtesy of* Osamu Nakashima, MD, Department of Pathology, Kurume University School of Medicine, Japan.)

and appear as hyperintense reticulations or areas (ie, confluent fibrosis)[33] compared with the surrounding hepatic parenchyma (**Fig. 12**). A recent study has shown the usefulness of double-contrast–enhanced MR imaging (sequential administration of SPIO and a gadolinium-based contrast agent) in the detection of liver fibrosis architecture. The investigators noted that the combination of these contrast agents was synergistic, and demonstrated liver fibrosis with greater clarity than could be achieved with either agent alone.[34]

Hepatobiliary-specific contrast agents such as mangafodipir trisodium (Mn-DPDP), gadobenate dimeglumine (Gd-BOPTA), and Gd-EOB-DTPA are taken up by functioning hepatocytes and excreted in the bile. The paramagnetic properties of these agents cause shortening of the longitudinal relaxation time (T1) of the liver and biliary tree. In visual analysis of images enhanced by Mn-DPDP, lower or heterogeneous enhancement areas are observed in cirrhotic liver, and it is considered that these areas contain the fibrous zone, indicating reticulation, confluent, and hepatocyte necrosis.[35,36] In the authors' experience, images enhanced by Gd-EOB-DTPA frequently show similar findings in cirrhotic liver, and this agent may also distinctly demonstrate liver fibrosis, such as fibrous septa, bridges (**Fig. 13**), and confluent fibrosis (see **Fig. 13**) (**Table 3**).

Emerging functional MR imaging techniques for fibrosis

Recently, several novel techniques for the assessment of liver fibrosis have been proposed, including MR elastography, diffusion-weighted MR imaging, and MR spectroscopy. MR elastography is a phase contrast-based MR imaging technique for direct visualization and quantitative measurement of propagating mechanical shear waves in biologic tissue.[37] Recent studies in patients with a spectrum of liver disease types have shown that liver stiffness as measured with MR elastography increases as the stage of fibrosis advances. The difference in stiffness between patients with early stages of fibrosis (F0 vs F1 vs F2) are small, with overlap between groups, but those between groups at higher stages (F2 vs F3 vs F4) are large, with little overlap.[38] Evaluation of the reproducibility and validity of MR

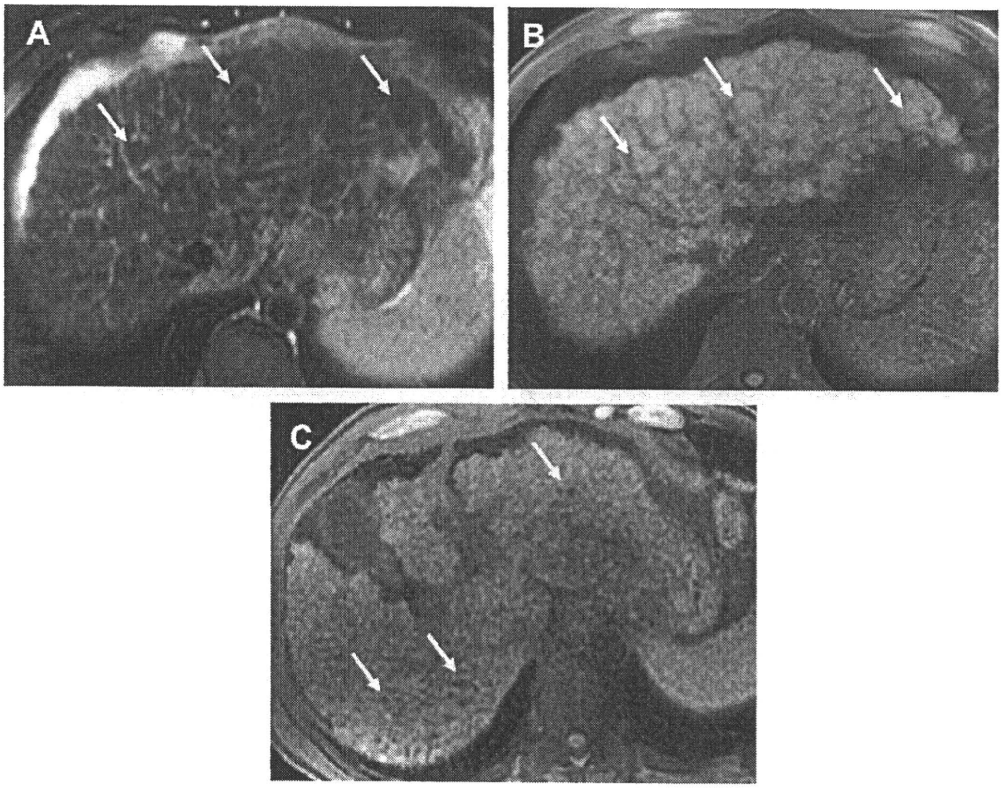

Fig. 15. Innumerable regenerative nodules have varying signal intensity, appearing isointense to hypointense on a T2-weighted fat-saturated TSE image (*A*) (*arrows*) and isointense to hyperintense on a T1-weighted fat-saturated 3D GRE image (TR/TE = 3.6/1.7 ms, flip angle = 15°) (*B*) (*arrows*). Hemosiderin deposition is common in regenerative nodules (siderotic nodules), producing such specific imaging features as hypointensity on T1-weighted fat-saturated 3D GRE image (*C*) (*arrows*).